LA-UR 00-4592

High-Brightness Electron Beam Production, Transport, and Measurement

Bruce E Carlsten

Los Alamos National Laboratory
Los Alamos, NM 87544

Abstract. This paper will review some of the recent developments in the area of high-brightness electron beams. Most of the paper will be devoted to emittance compensation concepts relating to high-brightness beam production in photoinjectors. Recent interpretation of emittance compensation and the residual emittance after compensation in terms of wave breaking has provided valuable insights into the process. Wave breaking also appears to have an influence on emittance growth and halo production in transport lines, which we will briefly discuss. There has been advances in understanding the emittance growth of bunches in circular motion, particularly related to the cancellation of longitudinal and transverse energy-independent forces. Finally, some non-intercepting bunch length and emittance diagnostic approaches will be reviewed.

INTRODUCTION

The following three sections review recent advances in emittance compensation, beam transport, and beam diagnostics, respectively. Due to the relatively large size of the high-brightness beam field due to its evolving maturity, a comprehensive review is not possible. Rather, the emphasis in this paper will be to review conceptual advances that have occurred recently that provide deeper fundamental understanding into some of the more critical aspects of high-brightness electron beam production, transport, and measurement.

A major insight in understanding emittance compensation was established with the introduction of using wave-breaking concepts to describe the final, residual emittance. These same concepts are applicable to a wide range of high-brightness electron beam dynamics, not just beam production from photoinjectors. Additionally, we can estimate the threshold initial emittance that leads to wave breaking and rapid thermalization in the first betatron period for high-brightness beams.

The next section will describe some aspects of high-brightness beam transport. The emphasis will primarily be on emittance preservation in bending systems. Recent work has demonstrated a remarkable cancellation between the energy-independent transverse and longitudinal forces. This cancellation is related to the cancellation of the centrifugal space-charge force with the beam's potential depression for DC beams. For periodic focusing channels, there is a halo and emittance growth mechanism related to the wave-breaking concepts of the earlier section.

In the final section, we will review some nonintercepting diagnostic developments. The transverse electric field from a short electron bunch has been measured via the phase shift of a laser beam in a crystal, which directly gives the wake field from that bunch, and potentially the bunch profile. Also recently, both the horizontal and vertical emittances have been measured with non-intercepting beam-position monitors.

DISCLAIMER

DISCLAIMER

Portions of this document may be illegible in electronic image products. Images are produced from the best available original document.

A final diagnostic which is very attractive is to use a chicane to rotate the beam's longitudinal phase space to directly obtain the bunch's longitudinal shape.

WAVE BREAKING AND EMITTANCE COMPENSATION

Emittance compensation has been used for over a decade to reduce the emittance from rf photoinjectors[1]. This emittance reduction is easy to understand in terms of coherent transverse plasma oscillations[2]. In Fig. 1 we see a typical plot of normalized emittance and beam size as a function of axial position[3].

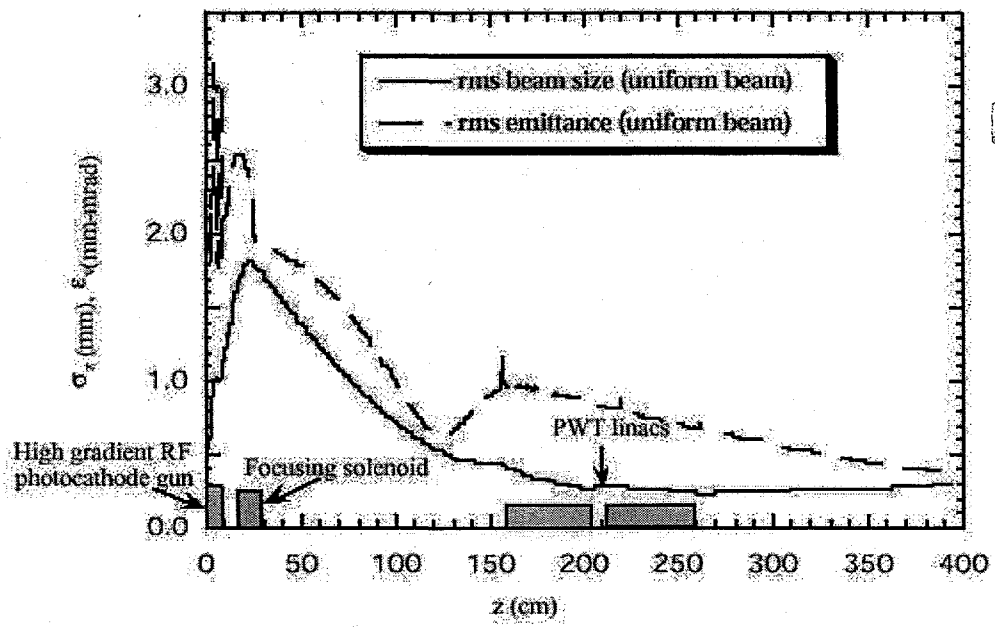

FIGURE 1. Simulation results of beam profile and emittance from a photoinjector design using an emittance-compensating solenoid and two PWT standing wave accelerator sections, from reference 3.

A nonuniform or bunched beam will undergo emittance oscillations due to the fact that the radial force is not simply proportional to radius everywhere. For a non accelerating beam, the radial equation of motion is:

$$\sigma'' + K\sigma - K_s/\sigma = 0 \qquad (1)$$

where σ is the transverse coordinate of a particle in a slice of the beam at a normalized radius ζ, K is a normalized focusing and $K_s = 2I(r)/I_A\gamma^3\beta^3$ is the normalized space-charge force, where $I(\zeta)$ is the current within radius ζ, γ is the beam's relativistic mass factor, β is its velocity normalized to the speed of light, and the primes refer to an axial derivative. We will assume that the beam motion is very nearly laminar, and that ζ is a constant for each particle.

The equilibrium particle orbit is given by $\sigma_{eq} = \sqrt{K_s/K}$, and we expand the orbits about this equilibrium position:

$$\sigma(\zeta,z)=\sigma_{eq}(\zeta,z)+\delta(\zeta,z) \quad . \tag{2}$$

Then, to first order the radial equation of motion becomes

$$\delta''(\zeta)+2K\delta(\zeta)=0 \quad . \tag{3}$$

This simple expression tells us that all particles will oscillate at the same frequency (to lowest order), and that any emittance growth due to a spread in phase-space angles from these oscillations will vanish every half-oscillation period. Even though this oscillation period only depends on the external focusing force, we will still refer to these oscillations as coherent transverse plasma oscillations. In Fig. 2 (also from reference 3), we see the area in phase space defined by three particles initially at the same radius, but with three different equilibrium positions, due to different space-charge forces λ. Each of the particles have a circular orbit, which is traversed clockwise. Each orbit takes nearly the same time to complete, as seen in Eqn. (3). The triangle shown in Fig. 2 is the area containing all three particles after a quarter oscillation period. Note that after both a half and a full oscillation period that the triangle collapses to zero volume. If $x-x'$ phase space was plotted instead of $r-r'$, the area would include another triangle with both x and x' symmetry on the left side of the $x=0$ axis, giving the phase-space area the appearance of a bow-tie.

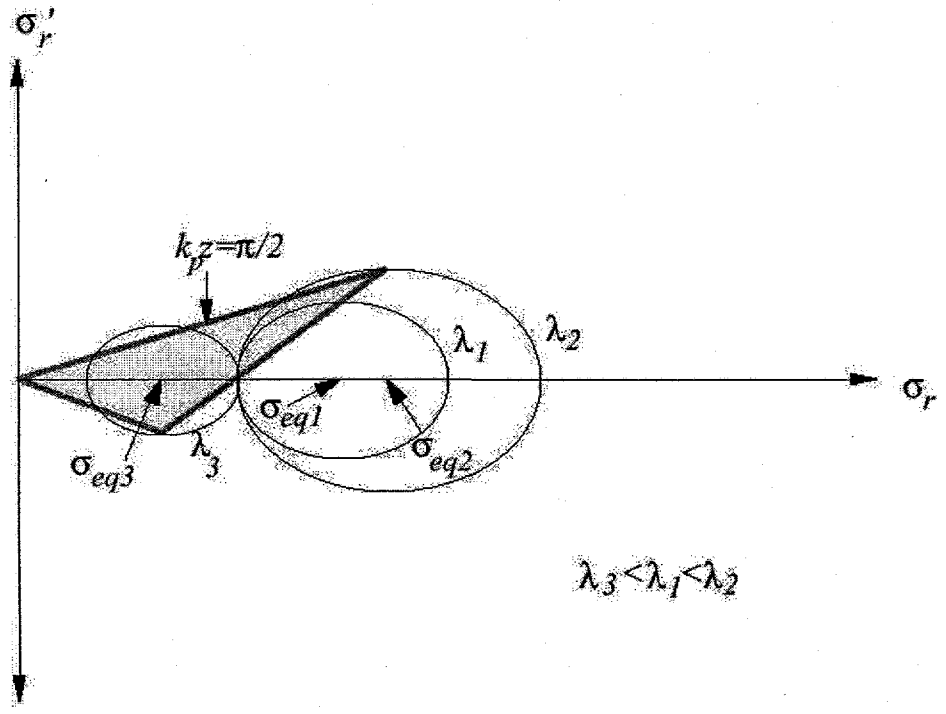

FIGURE 2. Formation of the "bow-tie" in phase space, outlined from three particles with the same initial positions, but with different equilibrium orbits (from reference 3).

Related emittance oscillations can be seen in many other areas of beam physics. The oscillations can be introduced by either radial or longitudinal nonlinearities. In Fig. 3, we plot emittance oscillations for a drifting 4 MeV, 4 kA, rms matched electron beam with zero initial emittance but with a nonuniform initial density distribution. The initial transverse kinetic energy of this beam is zero, but at the first emittance maximum, all the excess potential energy from the nonuniform density distribution has

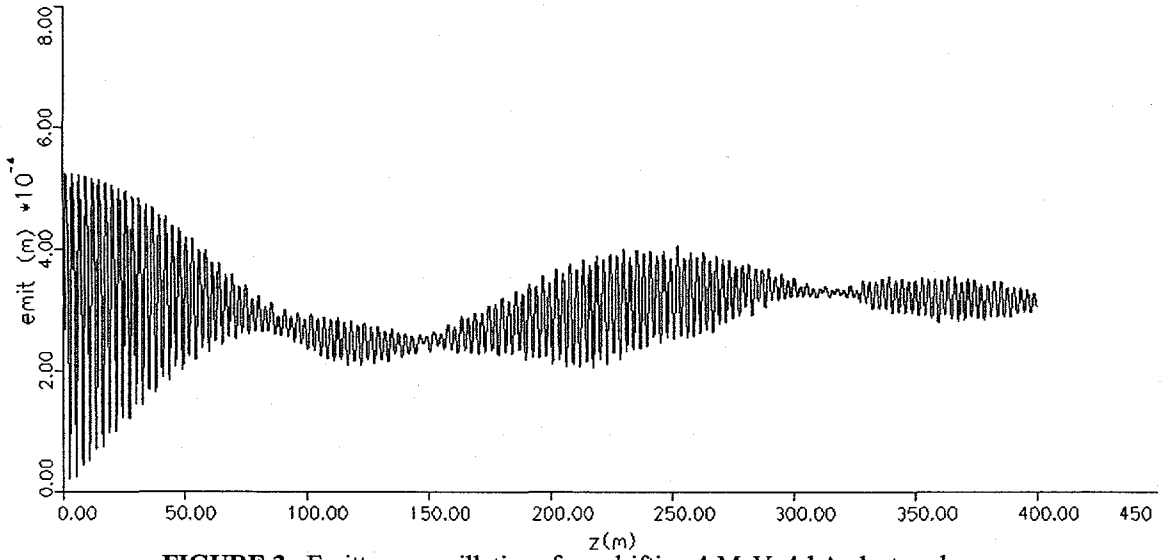

FIGURE 3. Emittance oscillations for a drifting 4-MeV, 4-kA electron beam.

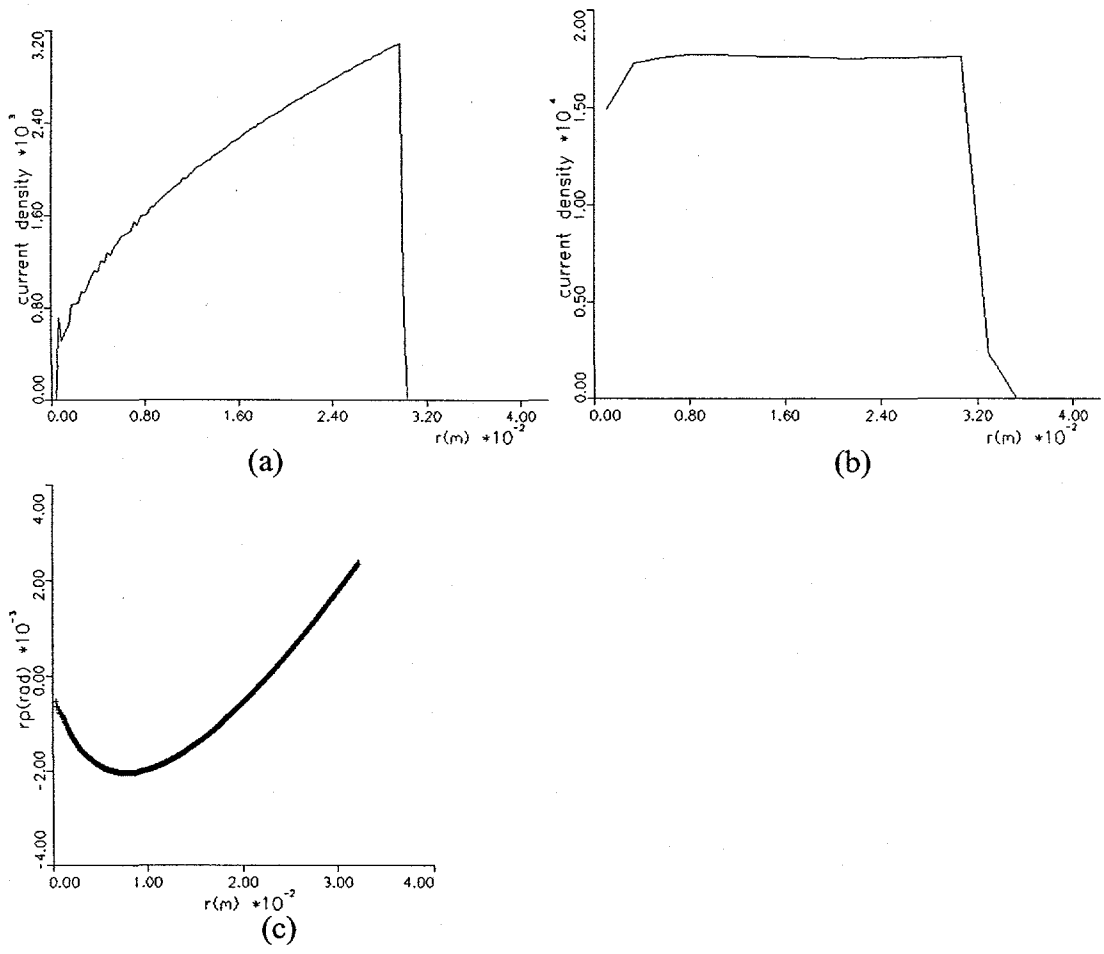

FIGURE 4. (a) Initial density distribution for the case shown in Fig. 3, (b) density profile at the first emittance maximum, and (c) phase space distribution at the first emittance maximum.

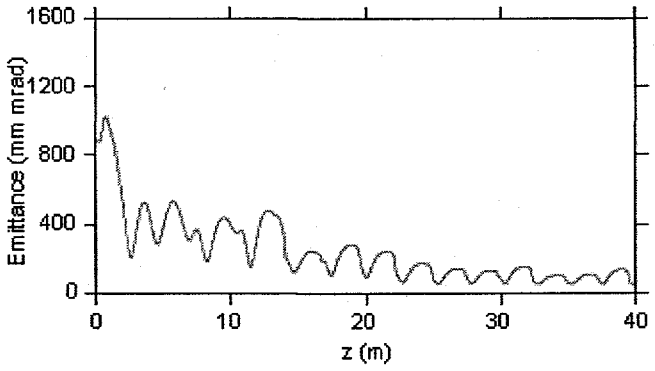

FIGURE 5. Normalized, 90% emittance evolution for 4-kA induction accelerator, showing emittance oscillations due to coherent transverse plasma oscillations.

been transferred into kinetic energy. Both the initial emittance maximum and the final emittance can be predicted from initial excess nonlinear field energy. For this case, the damping mechanism is from the spread of second-order frequencies. In general, though, thermalization results from wave breaking, where the $x-x'$ correlation in phase space becomes multivalued and the beam loses laminarity. Thermalization from wave breaking occurs relatively quickly, on the order of a half betatron period for mixing to occur.

In Fig. 4 we plot the initial density profile corresponding to the initial conditions of Fig. 3 (a), and the density profile (b) and the transverse phase space (c) at the first emittance maximum. These plots verify that the initial excess potential energy has been transferred into transverse kinetic energy. Note that the beam is rms matched, with a fixed point in phase space at the rms beam radius.

In Fig. 5 we see many of these emittance oscillations in a simulation of a 20-MeV, 4-kA induction linac, in which the pulse length is essentially DC. For the case of an rf photoinjector, there is typically only one emittance oscillation (and one-half of a transverse plasma oscillation) due to the rapid acceleration. For this simulation, nonlinear radial focusing in the diode and nonlinear radial space-charge forces induces the emittance oscillations.

With acceleration, the equations become more complex but the physics is essentially the same. The radial equation of motion is now:

$$\sigma'' + \sigma' \frac{\gamma'}{\gamma} + \sigma K \left(\frac{\gamma'}{\gamma \sin \phi} \right)^2 - \frac{K_s}{\sigma \gamma^3} = 0 \tag{4}$$

where ϕ is the rf phase angle of the bunch. With a Cauchy transform (using $y = \ln \gamma$)[2] this becomes

$$\frac{d^2 \sigma}{dy^2} + \Omega^2 \sigma = \frac{S e^{-y}}{\sigma} \tag{5}$$

where Ω has to do with focusing and the synchronous phase and $S(\zeta) = K_s(\zeta)/\gamma'^2$, which is a space-charge parameter. Reference 2 pointed out this equation has an exact solution

$$\sigma_{eq} = \sqrt{\frac{S}{\frac{1}{4}+\Omega^2}}\, e^{-y/2} \tag{6}$$

and the oscillations about this orbit (the invariant envelope) have (to first order) the same period. Although this solution has the same form as that for the coasting beam, there is a difference – the phase of the oscillations are not initially locked as before.

We can see this from the solutions of a trajectory perturbed from the equilibrium trajectory by an amount δ_0 (now we are thinking about slices that are radially uniform but differ in current longitudinally):

$$\begin{aligned} \sigma &= \sqrt{\frac{S/\gamma}{\frac{1}{4}+\Omega^2}} + \delta_0 \cos(\omega \ln\gamma + \theta) \\ \sigma' &= -\frac{\gamma'}{2}\sqrt{\frac{S/\gamma^3}{\frac{1}{4}+\Omega^2}} - \delta_0 \frac{\omega\gamma'}{\gamma}\sin(\omega \ln\gamma + \theta) \end{aligned} \tag{7}$$

The phase of these oscillations is clearly more complicated, and one can achieve better alignment of the slices if there is some flexibility of the initial conditions at the cathode (some initial divergence or rf focusing)

So far we have been talking about *laminar* coherent transverse plasma oscillations. The beam can become nonlaminar either radially or longitudinally if the current density drops sufficiently low[4]. In an axial slice of the bunch, the outer electrons are not repelled enough by the space charge force (for rms matched focusing) if the beam density drops to a point somewhat less than ½ of the average density out to that point. If the outer particles are not repelled, they cross into the core of the beam, forming wave breaking. In Fig. 6(a) we see the beam's phase space exiting a diode for the case in the previous figure (4-kA and 3.5-MeV beam). Some amount of modest wave breaking is already seen at this location, due to nonlinear electrostatic and magnetic focusing. This simulation uses the diode simulation code EGUN[5], and assumes that the initial beam emittance (at the cathode) is zero. As the beam travels downstream in the accelerator, the particles which have wave broken (and thus have nonlaminar trajectories) pass through the core of the beam, forming a halo, as seen in Fig. 6(b). During the focusing part of each radial oscillation, additional particles at the edge of the beam's radial distribution wave break. Eventually, the wave broken particles oscillate about the 2:1 resonance, forming a ring in phase space around the laminar particles defining the core (shown in Fig. 6(c)).

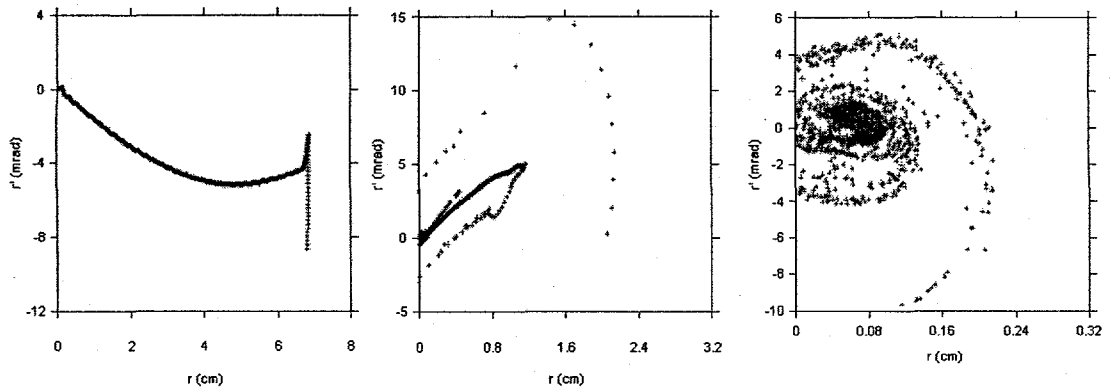

FIGURE 6. (a) Initial phase space distribution after the electron diode, (b) wave breaking particles passing through the beam core forming a halo early on, and (c) final evolved distribution with wave breaking particles spiraling about the 2:1 resonance.

At this point we know that emittance oscillations will occur if the beam either has an initial emittance or some initial density profile mismatch. If no wave breaking occurs, these oscillations will persist for very long times and distances (see Fig. 3 for example). However, if the beam wave breaks, the thermalization will occur much faster – essentially at the rate that the particles wave break. Note that the characteristic time scale for wave breaking is a radial compression, or about a ¼ betatron period. This time scale has been empirically described before[6]. Although we can not make general statements about the rate of wave breaking for particles in transport, we can easily estimate a characteristic emittance which will always lead to significant wave breaking in the first betatron period. Wave breaking of about ½ the particles will occur for a uniform density beam with an initial emittance exceeding[7]

$$\varepsilon_{w-b} = 4r_e\sqrt{(I/I_A)/\gamma\beta} \quad . \tag{8}$$

By definition, high-brightness electron beams are under this limit, and do not undergo immediate, large-scale wave breaking. However, rapid phase-space mixing is common for ion beams (this emittance threshold is only 0.2 mm mrad for a 1-GeV, 100-mA, 1-mm radius hydrogen beam). This consideration explains why high-brightness electron beams do not thermalize like ion beams.

In an rf photoinjector, the radial nonlinearities are often less important than the time dependence of the current profile of the pulse. For this case, the ends of the electron bunch are not rms matched, and the emittance will oscillate from the mechanism shown in Fig. 2. The emittance thermalization will occur fairly rapidly as the head and tail slices with lower current will exhibit behavior essentially the same as if they wave broke relative to the slices near the center of the bunch. However, as long as the individual slices do not wave break, this emittance is still theoretically recoverable. Most importantly, for longitudinal current variations and no radial nonlinearities, there is no excess of nonlinear free energy which leads to a nonzero thermalized emittance. For the case of the rf photoinjector, if the phase of the emittance oscillations is properly matched, the emittance can theoretically vanish at the beam's application in the absence of wave breaking.

In Fig. 7 (from reference 3) we see phase-space plots from a simulation of an rf photoinjector, with no radial nonlinearities and with an initially radially uniform beam density, using the accelerator simulation code PARMELA[8]. The characteristic bow-tie shape is very evident in the $x-x'$ phase space shown in Fig. 7(a). In Fig. 7(b) we see the $x-z$ configuration space, which shows that the head and tail slices of the bunch have been overfocused (due to their lower space-charge forces). In Fig. 7(c) we see the $x-x'$ phase space of the distribution with $|\delta z| < 0.1\,\text{mm}$. Note that the core still has a bow-tie distribution, and the spread in the bow-tie angles is due to the second order dependence on the oscillation frequency about a given slice's equilibrium orbit. The effect of the head and tail particles in Fig. 7(a) show some small additional wave breaking characteristics.

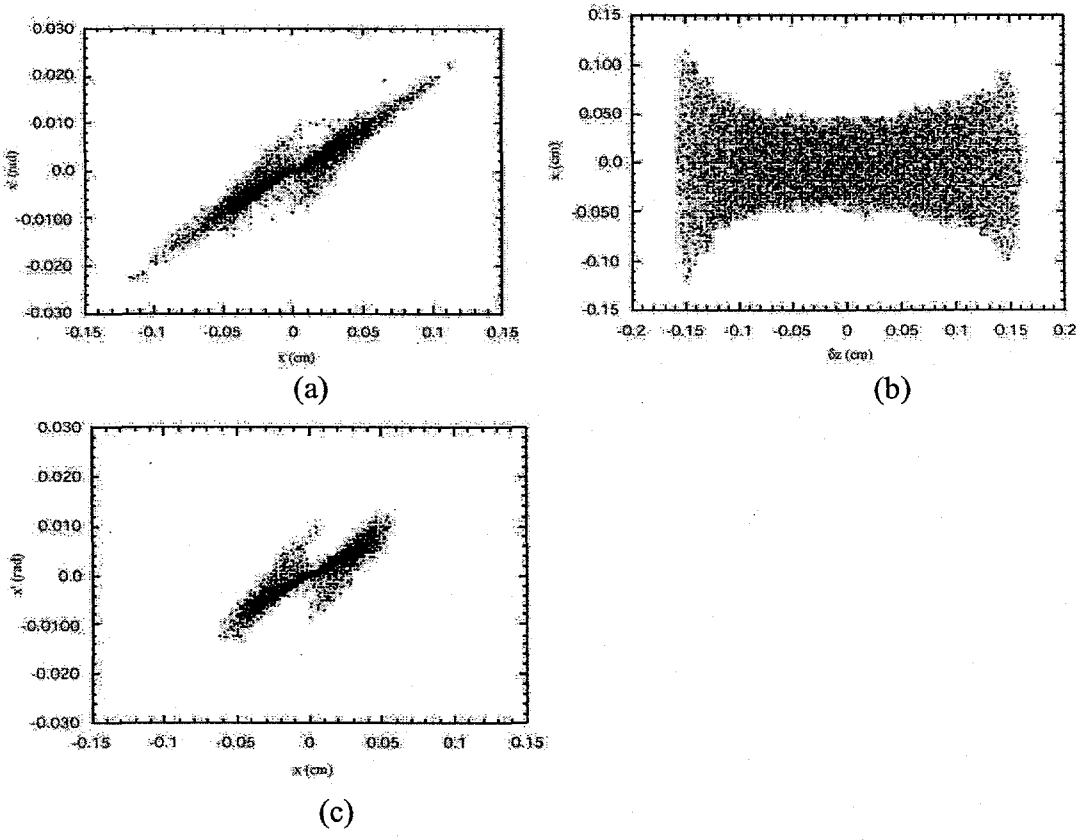

FIGURE 7. (a) Phase space for entire beam, (b) x-z correlation, (c) phase space for core of beam (from reference 3)

In Fig. 8, also from reference 3, we see the same plots for the same accelerator design, but with an initially nonuniform radial beam distribution. Now Figs. 8(a) and 8(c) are more similar, and demonstrate a subdistribution with strong wave breaking characteristics (the horizontal distribution perpendicular to the bow-tie distribution). The emittance of this case is four times larger than the previous case, with much less pronounced emittance oscillations (more rapid thermalization).

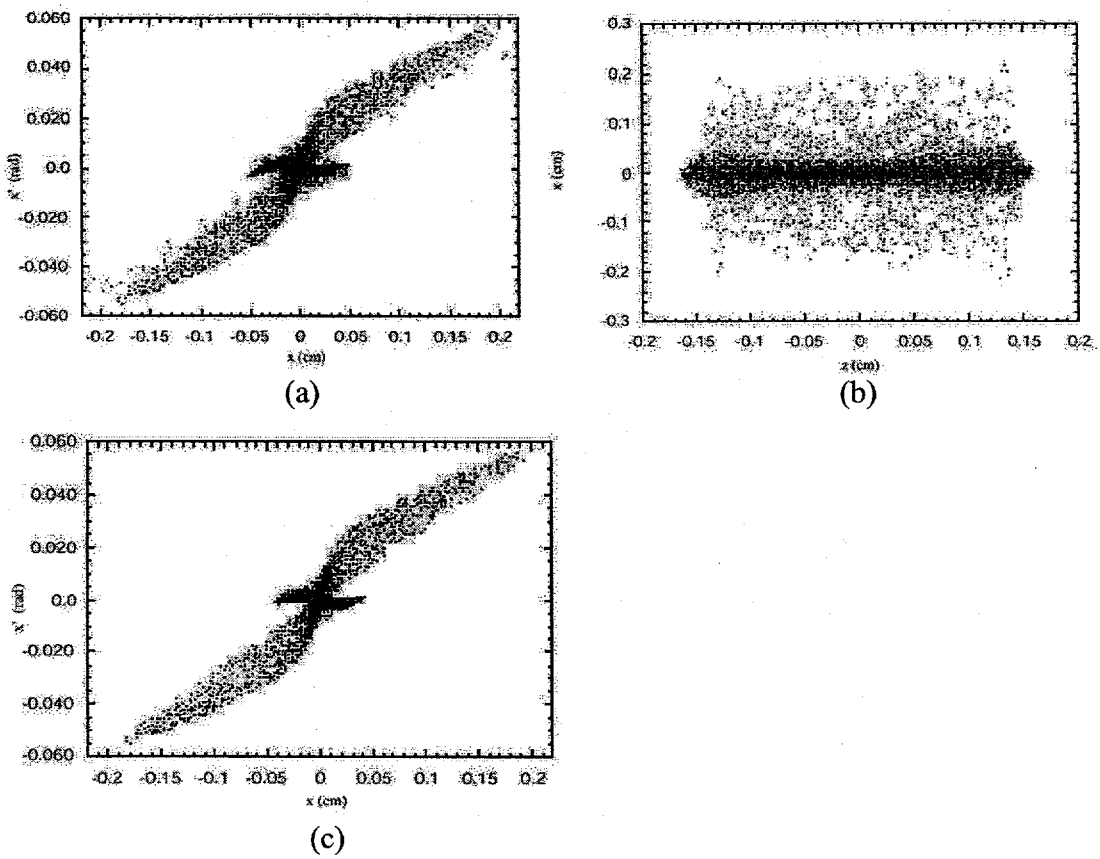

FIGURE 8. (a) Phase space for entire beam, (b) x-z correlation, (c) phase space for core of beam, for case showing radial wave breaking (from reference 3)

In practice, the rf emittance growth is not negligible, particularly at high frequencies. For many cases the rf emittance dominates, and is given by[9]

$$\varepsilon_{rf} = \frac{eE_o}{2\sqrt{2}m_o c^2} k^2 \sigma_x^2 \sigma_z^2 \quad . \tag{9}$$

This is probably the reason that L-band photoinjectors are competitive with higher frequency devices.

Timing stability for very high frequency rf photoinjector can be problematic[10]. The stability for W-band (90 GHz) photoinjectors is on the order of tens of fs, which is better than standard drive lasers can produce. One way around this is to use an essentially DC laser and bunch the electrons that get accelerated in an undulator[10]. Electrons from 65 degrees of phase get out of the gun (15 A, 30 pC in 2 ps at the cathode, and up to 70 A with 1.8 MeV energy at the exit). The energy spread is mostly linear, and the beam can be bunched to 600 A in the undulator, with about 1.5 mm mrad.

TRANSPORT ISSUES FOR HIGH-BRIGHTNESS ELECTRON BEAMS

We will review two recent developments in the transport of high-brightness electron beams. First, we will describe some recent work on halo production in periodically focused systems, where wave breaking can occur continually along the transport line The physics is different than for uniformly focused systems, and leads to a fuzzy separatrix. Second, we will review the emittance growth from coherent synchrotron radiation (CSR) effects in bends. This understanding is becoming quite mature, although there are still some loose ends.

Recent work[11] on periodic focusing channels show that the separatrix becomes fuzzy and particles can enter the 2:1 resonance that were initially in the core. Wang developed a new technique for stroboscopic plots for periodic focusing which reduces the flutter, and shows the separatrix becomes poorly defined. With varying focusing, particles can enter the 2:1 resonance (wave break) essentially anywhere along the beam line transport. Class I particles remain inside the core, Class II particles are outside the core but not in resonance with the core, Class III particles oscillate at ½ the core frequency (2:1 resonance), Class IV particles oscillate with large amplitudes, and Class V particles can be driven in and out of resonance by the periodic focusing and the flutter, an effect not found in uniform focusing cases. The action of the Class V particles can be described in terms of wave breaking from radial oscillations due to the periodic focusing.

There are several effects that can lead to beam brightness degradation for a beam traveling in a bend system. The first of these is if the optics are non-achromatic; the accelerator community knows how to avoid this and this is usually not a problem. There are also transverse space-charge forces which have a $1/\gamma^2$ scaling. There forces typically dominates at low energy and are also negligible at high energy. Finally, there are longitudinal space-charge forces which do not have the $1/\gamma^2$ scaling and the effects from these forces dominate at high energy. The resulting beam degradation can be exhitbited either as transverse emittance growth or energy spread. The energy independent longitudinal force has two parts, the coherent synchrotron radiation (CSR) which is a long range, radiative force, and the noninertial space-charge force (NISCF) which is short range and nonradiative.

The importance of these longitudinal forces is that they cannot be reduced by going to larger radius bends – the longitudinal forces (and resulting emittance growths) scales as $R^{1/3}$ and is independent of beam energy (at high enough energy)

The following derivation of the longitutinal space-charge forces in a bend clearly separates out the CSR and NISCF terms. The electric field from a line of charge is given by[12]:

$$E_\theta = -\frac{\partial A_\theta}{\partial t} - \frac{1}{r}\frac{\partial \phi}{\partial \theta} \tag{10}$$

where

$$\phi = \frac{1}{4\pi\varepsilon}\int_{\zeta_r}^{\zeta_f} \frac{\lambda}{r_{ret} - \vec{r}_{ret}\cdot\vec{u}_{ret}/c} d\zeta$$
$$A_\theta = \frac{1}{4\pi\varepsilon c}\int_{\zeta_r}^{\zeta_f} \frac{\lambda\beta\cos\zeta'}{r_{ret} - \vec{r}_{ret}\cdot\vec{u}_{ret}/c} d\zeta \quad . \tag{11}$$

Explicit calculation for a uniform density line of charge gives:

$$E_\theta = \frac{\lambda}{4\pi\varepsilon}\frac{1}{r_{ret} - \vec{r}_{ret}\cdot\vec{u}_{ret}/c}\left(\frac{1}{\gamma^2} - \beta^2\frac{x}{R} + \beta^2\frac{r}{R}(1-\cos(\zeta'))\right)\Bigg|_{\zeta_r}^{\zeta_f} \tag{12}$$

where the retarded time is given by

$$\frac{R^2}{\beta^2}(\zeta'-\zeta)^2 = \rho^2 + 2R(R+x)(1-\cos\zeta') \quad . \tag{13}$$

We see three terms on the right-hand-side of Eqn. (12), which we can identify as: (1) the "usual" $1/\gamma^2$ space-charge term (but not the same as for straight-line motion), (2) the noninertial space-charge force (NISCF), and (3) the coherent synchrotron radiation force (CSR)

There is also an energy independent transverse force, the centrifugal space-charge force (CSCF), which cancels the effect from the beam's potential depression[13]. We can easily see this cancellation for the DC case, starting with the approximation $\vec{A} = \left(0, \frac{\beta}{c}\phi, 0\right)$, and defining $x = r - R$, where R is bend radius. For the DC case, the radial force is

$$F_r = e\left(E_r + v_z B_\theta - v_\theta B_z\right) = e\left(-\frac{1}{\gamma^2}\frac{d\phi}{dr} + \beta^2\frac{\phi}{R}\right) \quad . \tag{14}$$

The radial equation of motion is given by

$$\frac{d}{dt}\gamma\dot{r} = \frac{\gamma v^2}{r} - \frac{evB_{ext}}{m} + \frac{e}{m}\left(-\frac{1}{\gamma^2}\frac{d\phi}{dr} + \beta^2\frac{\phi}{R}\right) \quad . \tag{15}$$

We expand to lowest order in R about the equilibrium orbit, defined by $0 = \frac{\gamma_0 v^2}{r} - \frac{evB_{ext}}{m} + \frac{e}{m}\beta^2\frac{\phi(0)}{R}$ and let $\gamma_1 = \gamma - \gamma_0$, and the radial equation of motion becomes

$$\ddot{x} = -\frac{\dot{\gamma}_1}{\gamma}\dot{x} + \frac{v^2}{R}\left(\frac{\gamma_1}{\gamma} - \frac{x}{R}\right) + e\beta^2\frac{\phi(x)-\phi(0)}{\gamma mR} - \frac{e}{\gamma^3 m}\frac{\phi(0)}{R} \quad . \tag{16}$$

Now $\gamma_1 = -e\frac{\phi(x)-\phi(0)}{mc^2}$ so the curvature term cancels the potential depression term, leaving

$$\ddot{x} = \frac{v^2}{R^2}x - \frac{e}{\gamma\ m}\frac{\phi(0)}{R}\left(\beta_t^2 - \frac{1}{\gamma^2}\right) \quad , \tag{17}$$

and the energy independent transverse space-charge term has vanished. The CSCF cancels the potential depression of the beam, leading to the surprising effect that the beam steers as if there was no potential depression of the beam. This effect has actually been experimentally verified[14].

Recently, R. Li[15] made important observation – for a bunched beam, the noninertial space charge force leads to a change in a particle's potential, which is canceled by the CSCF term! We can sketch this cancellation out (the derivation is similar to DC case, but now with time derivatives). The radial equation of motion is

$$\frac{d}{dt}\gamma m\dot{r} = e\left(\vec{E} + \vec{v}\times\vec{B}\right)_r + \frac{\gamma m v_\theta^2}{r} \tag{18}$$

Using $r = x + R$ and $\vec{E} = -\vec{\nabla}\phi - \dot{\vec{A}}$ we get

$$\gamma m\ddot{x} + \dot{\gamma}m\dot{x} = \frac{\gamma m v_\theta^2}{R+x} + e\frac{\partial}{\partial x}\left(-\phi - v_\theta A_\theta\right) - e\left(\frac{\partial}{\partial t} + \frac{v_\theta}{r}\frac{\partial}{\partial\theta}\right)A_r + e\frac{v_\theta A_\theta}{r} - ev_\theta B_{ext} \tag{19}$$

and with $ev_\theta B_{ext} = \frac{\gamma_o m v_\theta^2}{R}$ this becomes ($\gamma = \gamma_o + \gamma_1$)

$$\ddot{x} = \frac{v_\theta^2}{R}\left(\frac{\gamma_1}{\gamma_o} - \frac{x}{R}\right) + \frac{e}{m\gamma}\left(\frac{\partial}{\partial x}\left(-\phi - v_\theta A_\theta\right) - \frac{d}{dt}A_r + \frac{v_\theta A_\theta}{r}\right) \quad . \tag{20}$$

Using the azimuthal electric field,

$$\gamma_1 = \frac{e}{mc^2}\int\left(-\frac{1}{r}\frac{\partial}{\partial\theta}\phi - \dot{A}_\theta\right)ds = \frac{ev_\theta}{mc^2}\int\left(-\frac{1}{r}\frac{\partial}{\partial\theta}\phi - \frac{1}{v_\theta}\frac{\partial}{\partial t}\phi + \frac{1}{v_\theta}\frac{\partial}{\partial t}\phi - \dot{A}_\theta\right)dt$$

$$= \frac{ev_\theta}{mc^2}\int\left(-\frac{1}{v_\theta}\frac{d}{dt}\phi + \frac{1}{v_\theta}\frac{\partial}{\partial t}\phi - \dot{A}_\theta\right)dt \quad . \tag{21}$$

The radial equation of motion now becomes

$$\ddot{x} = -\frac{v_\theta^2 x}{R^2} + \frac{\beta_\theta^2 e}{\gamma_o Rm}\left(-\phi + \int\left(\dot{\phi} - v_\theta\dot{A}_\phi\right)dt\right) + \frac{e}{m\gamma}\left(\frac{\partial}{\partial x}\left(-\phi - v_\theta A_\theta\right) - \frac{d}{dt}A_r + \frac{v_\theta A_\theta}{r}\right) \tag{22}$$

or (to lowest order)

$$\ddot{x} = -\frac{v_\theta^2 x}{R^2} + \frac{e}{\gamma_o Rm}\left(\left(-\beta_\theta^2\phi + v_\theta A_\theta\right) + \beta_\theta^2\int\left(\dot{\phi} - v_\theta\dot{A}_\phi\right)dt + R\frac{\partial}{\partial x}\left(\left(-\phi - v_\theta A_\theta\right)\right)\right) \tag{23}$$

where the first term is geometric, the second is the CSCF and NISCF cancellation, the third is the CSR term and the fourth is the centripetal space-charge force.

HIGH-BRIGHTNESS BEAM DIAGNOSTICS

The main challenges of diagnostics for high-brightness beams is to measure extremely small bunch lengths and to measure very low emittances. Both measurements provide difficulties, as even the process of measuring the beam can change it. In general, the more promising diagnostics are nonintercepting. In this section, we will review three relatively new diagnostic ideas. First, we will review progress on measuring the beam emittance using the quadrupole moments from beam-position monitors (BPMs). Emittances as low as 10 mm mrad have been measured successfully with this technique to date. Next, we will describe measurements made on the transverse electric field induced by the passing of a short electron bunch. This technique promises to measure both wake impedances of specific accelerator components and even the bunch current profile. Finally, we will describe an intercepting bunch length diagnostic that uses a chicane to rotate the longitudinal phase space.

Measuring the emittance using a BPM was suggested in 1983[16] and was first demonstrated in 1999[17]. The technique uses a single BPM, shown in Fig. 9, and two quadrupoles.

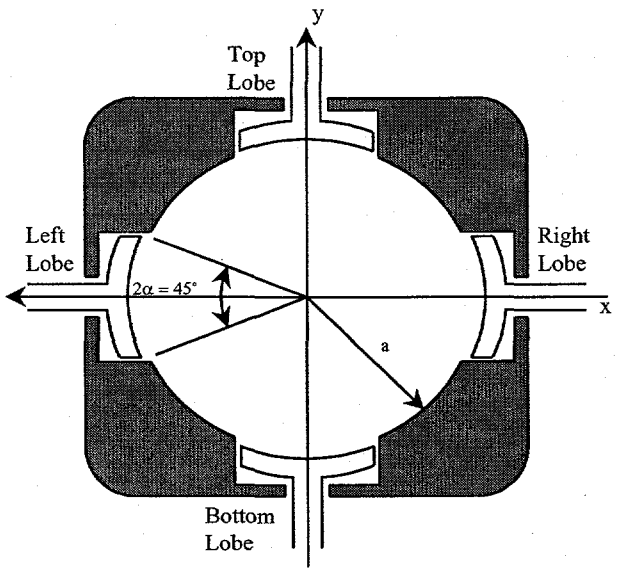

Fig. 9. Beam-position monitor schematic.

The technique is based on the fact that a BPM is sensitive to the second moment of the beam's distribution. The difference between the horizontal and vertical second moments is given by

$$\left\langle x^2 \right\rangle - \left\langle y^2 \right\rangle + \bar{x}^2 - \bar{y}^2 = a^2 \frac{\alpha}{\sin 2\alpha} \frac{A_R + A_L - A_T - A_B}{A_R + A_L + A_T + A_B} \tag{24}$$

where A_R, A_L, A_T and A_B are the signal amplitudes of the right, left, top and bottom electrodes of the BPM. The beam's phase space upstream of the quadrupole can be determined by inverting the relationship

$$\left\langle x^2\right\rangle_{BPM} - \left\langle y^2\right\rangle_{BPM} = (R_{11})^2\left\langle x^2\right\rangle_q + 2R_{11}R_{12}\left\langle xx'\right\rangle_q + (R_{12})^2\left\langle x'^2\right\rangle_q - (R_{33})^2\left\langle y^2\right\rangle_q - 2R_{33}R_{34}\left\langle yy'\right\rangle_q - (R_{34})^2\left\langle y'^2\right\rangle_q, \quad (25)$$

where the BPM subscript refers to the BPM location and the q subscript to just upstream of the quadrupole. The constants R_{jk} are from the transfer matrix for the focusing channel between the upstream point and the BPM:

$$\bar{\bar{\mathbf{R}}} = \begin{bmatrix} R_{11} & R_{12} & 0 & 0 \\ R_{21} & R_{22} & 0 & 0 \\ 0 & 0 & R_{33} & R_{34} \\ 0 & 0 & R_{43} & R_{44} \end{bmatrix}. \quad (26)$$

Tremendous progress has been made in using electro-optical effects to time-resolve the transverse electric field from a passing bunch of charge. One such experiment is taking place at Fermilab A $LiTaO_3$ electro-optic crystal is used to generate a phase shift in a laser beam due to the induced electric field from a passing electron bunch in a chamber. So far, the transverse field has been resolved with a time resolution of about 10 ps. Because the diagnostic is in a cross, the wake potential is actually measured; if the diagnostic were in a smooth pipe, the current profile of the bunch would be found.

The idea of the intercepting bunch-length diagnostic[19] is to pass the beam through a chicane followed by an off-phase accelerating structure with the following total transfer matrix and mapping from initial to final longitudinal phase space:

$$\begin{pmatrix} 1 & 0 \\ \alpha & 1 \end{pmatrix}\begin{pmatrix} 1 & \delta \\ 0 & 1 \end{pmatrix}\begin{pmatrix} t \\ E \end{pmatrix} = \begin{pmatrix} t+\delta E \\ \alpha t + (1+\alpha\delta)E \end{pmatrix}. \quad (27)$$

If $\alpha\delta = -1$, then the final energy of a particle only depends on its initial time, $E_{final} = \alpha t_{initial}$ and the bunch profile can be measured in a spectrometer. An experiment[20] measured the bunch current profile of an initially 19 MeV beam (accelerated to 27 MeV in the final accelerating structure) with 260 fs resolution. This technique is capable of a resolution of 16 fs for a beam of 100 MeV beam with a 10 MeV section at 10 GHz.

REFERENCES

[1] B. E. Carlsten, Particle Accelerators **49**, 27 (1995).
[2] L. Serafini and J. B. Rosenzweig, Phys. Rev. E **55**, 7565 (1997).
[3] S. G. Anderson and J. B. Rosenzweig, Phys. Rev. ST Accel. Beams **3**, 094201 (2000).
[4] O. A. Anderson, Particle Accelerators **21**, 197 (1987).
[5] W. B. Herrmannsfeldt, Linear Accelerator and Beam Optics Codes Workshop, San Diego, (1998).
[6] M. Reiser, *Theory and design of charged particle beams* (John Wiley and Sons, Inc., New York, 1994), Chap. 6
[7] B. E. Carlsten, Phys. Rev. E **60**, 2280 (1999).

[8] L. Young, Los Alamos National Laboratory, private communication.
[9] K.J. Kim, Nucl. Instrum. Meth. Phys. Res. **A275**, 210 (1989).
[10] D. T. Palmer and M. J. Hogan, 1999 Particle Accelerator Conference, IEEE Catalog Number 99CH36366, New York, 1997, (1999).
[11] T.S. F. Wang, Phys. Rev. E **61**, 855 (2000).
[12] W. Panofsky and M. Phillips, *Classical electricity and magnetism* (Addison-Wesley Publishing Company, Inc., Reading, MA, 1955)
[13] E. P. Lee, Particle Accelerators **25**, 241 (1990).
[14] P. Allison, D. C. Moir, and G. Sullivan, 1997 Particle Accelerator Conference, IEEE Catalog Number 97CH36167, Vancouver, 1144, (1997).
[15] R. Li, Thomas Jefferson National Accelerator Facility, private communication, 1999.
[16] R. Miller, J. Clendenin, M. James, and J. Sheppard, 12th International Conference on High Energy Accelerators, Fermilab, 602, (1983).
[17] S. J. Russell, Rev. Sci. Instrum. **70**, 1362 (1999).
[18] Michael Fitch, Fermilab, private communication, 2000.
[19] E. R. Crosson, K. W. Berryman, B. A. Richman, T. I Smith, and R. L. Swent, AIP Conference Proceedings **367**, 397 (1995).
[20] K. N. Ricci, T. I. Smith, and E. R. Crosson, Nucl. Meth. Instrum. Phys. Res. **A429**, II-61 (1999).